

Supplementary Information

Triboelectrification Behaviors of Inorganic $\text{Cs}_{1-x}\text{A}_x\text{PbBr}_3$ Halide Perovskites toward Enriching Triboelectric Series

Yudi Wang,^a Xiya Yang,^{a,*} Wenkai Xu,^a Xueping Yu,^a Jialong Duan,^a Yanyan
Duan,^b and Qunwei Tang^a

^a Institute of New Energy Technology, College of Information Science and
Technology, Jinan University, Guangzhou 510632, PR China;

^b State Centre for International Cooperation on Designer Low-Carbon and
Environmental Material (SCICDLCEM), School of Materials Science and Engineering,
Zhengzhou University, Zhengzhou 450001, PR China;

E-mail address: xiyayang@jnu.edu.cn

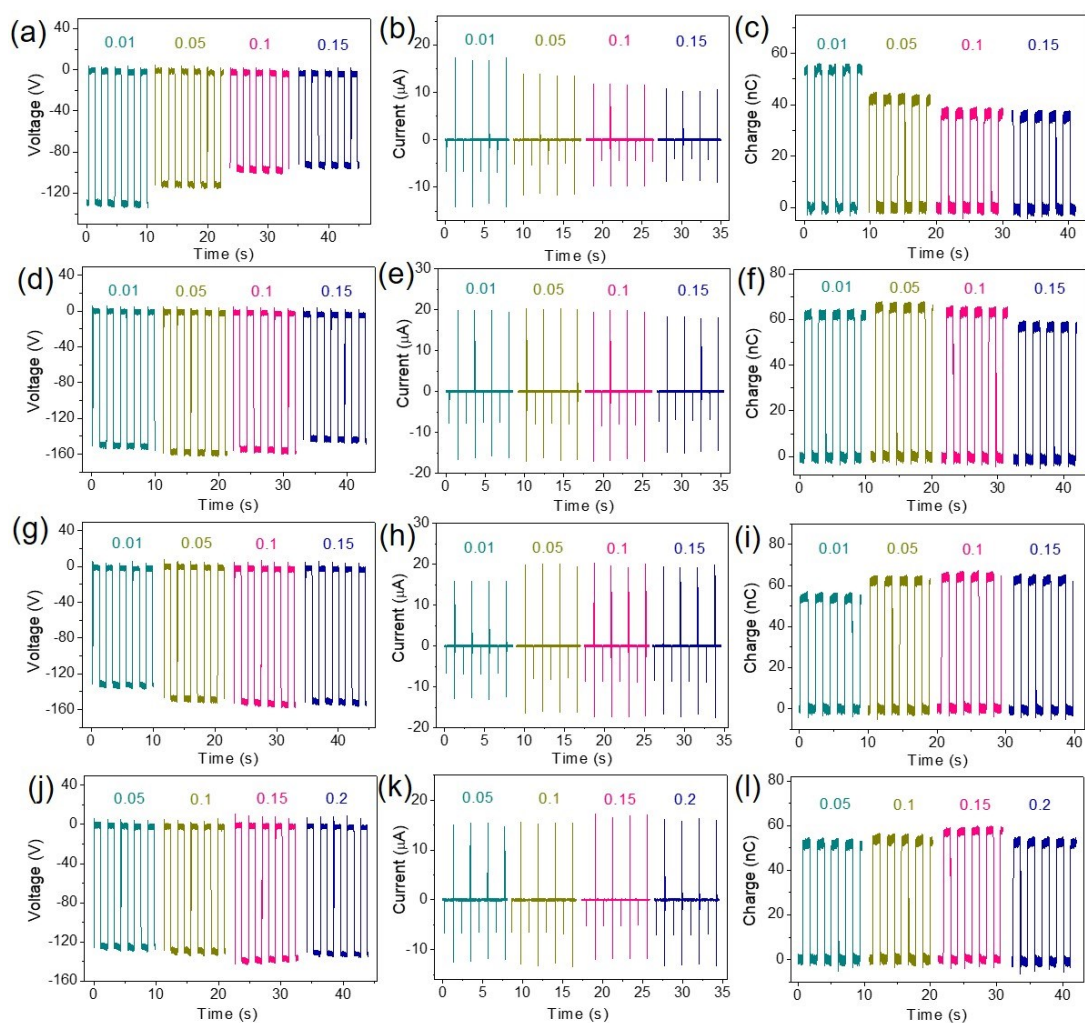


Figure S1. Triboelectric (a, d, g, j) voltage, (b, e, h, k) current, and (c, f, i, l) charge outputs of the perovskites doped with (a-c) Li^+ , (d-f) Na^+ , (g-i) K^+ , and (j-l) Rb^+ at various doping contents.

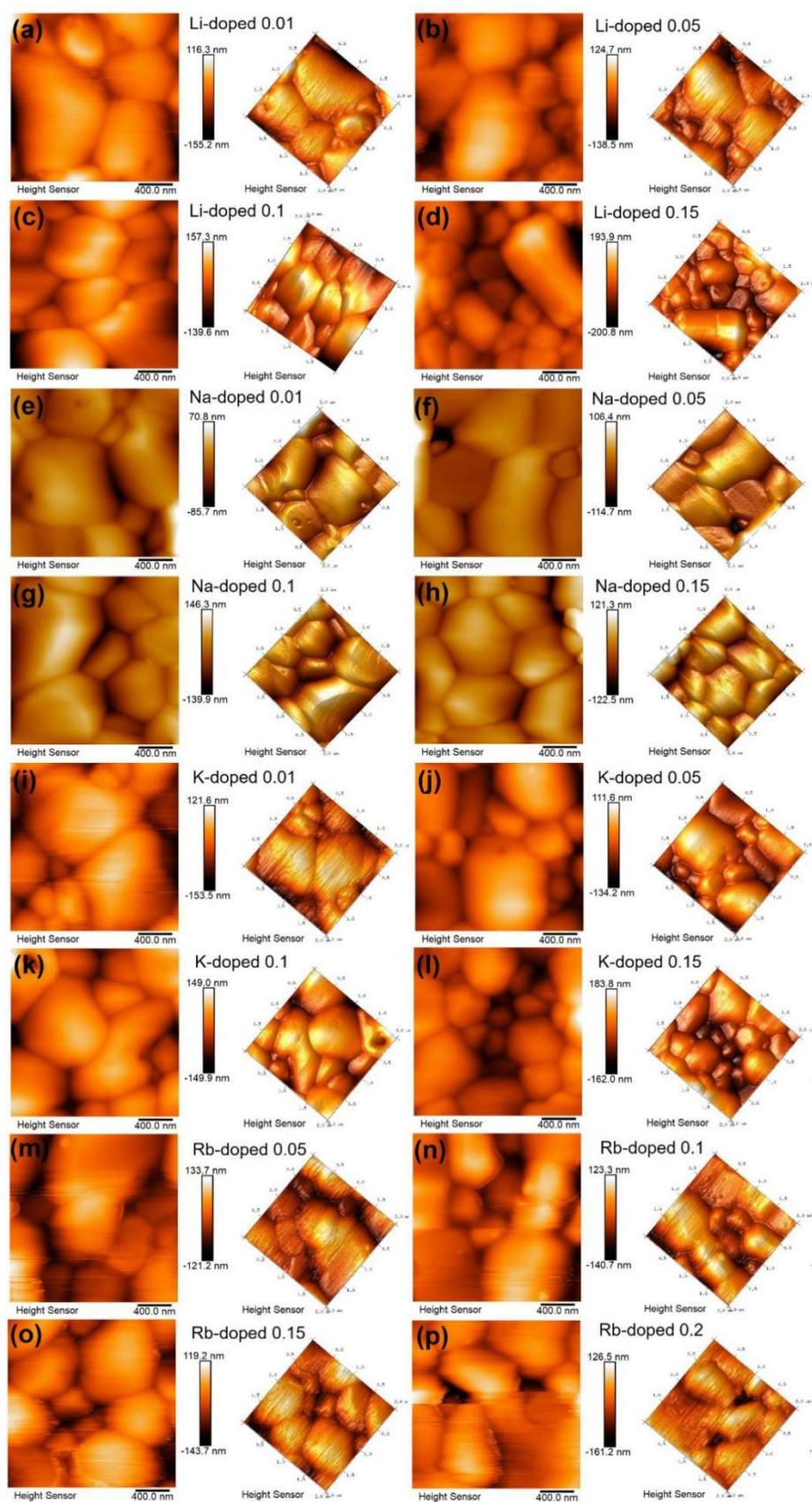


Figure S2. AFM characterizations of surface roughness of $\text{Cs}_{1-x}\text{A}_x\text{PbBr}_3$ films with increased (a-d) Li^+ , (e-h) Na^+ , (i-l) K^+ , (m-p) Rb^+ doping contents.

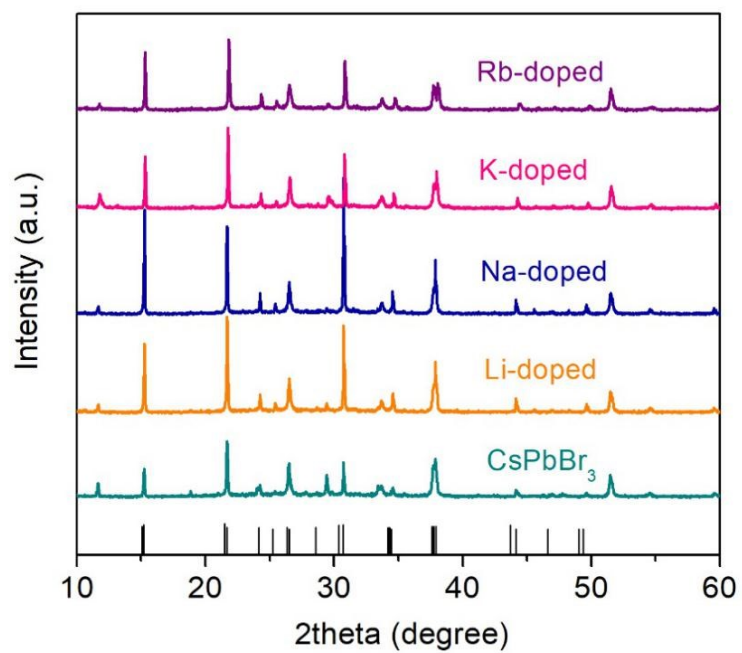


Figure S3. XRD patterns of pristine CsPbBr₃ and Cs_{1-x}A_xPbBr₃ perovskite films and the standard CsPbBr₃ perovskite lattice.

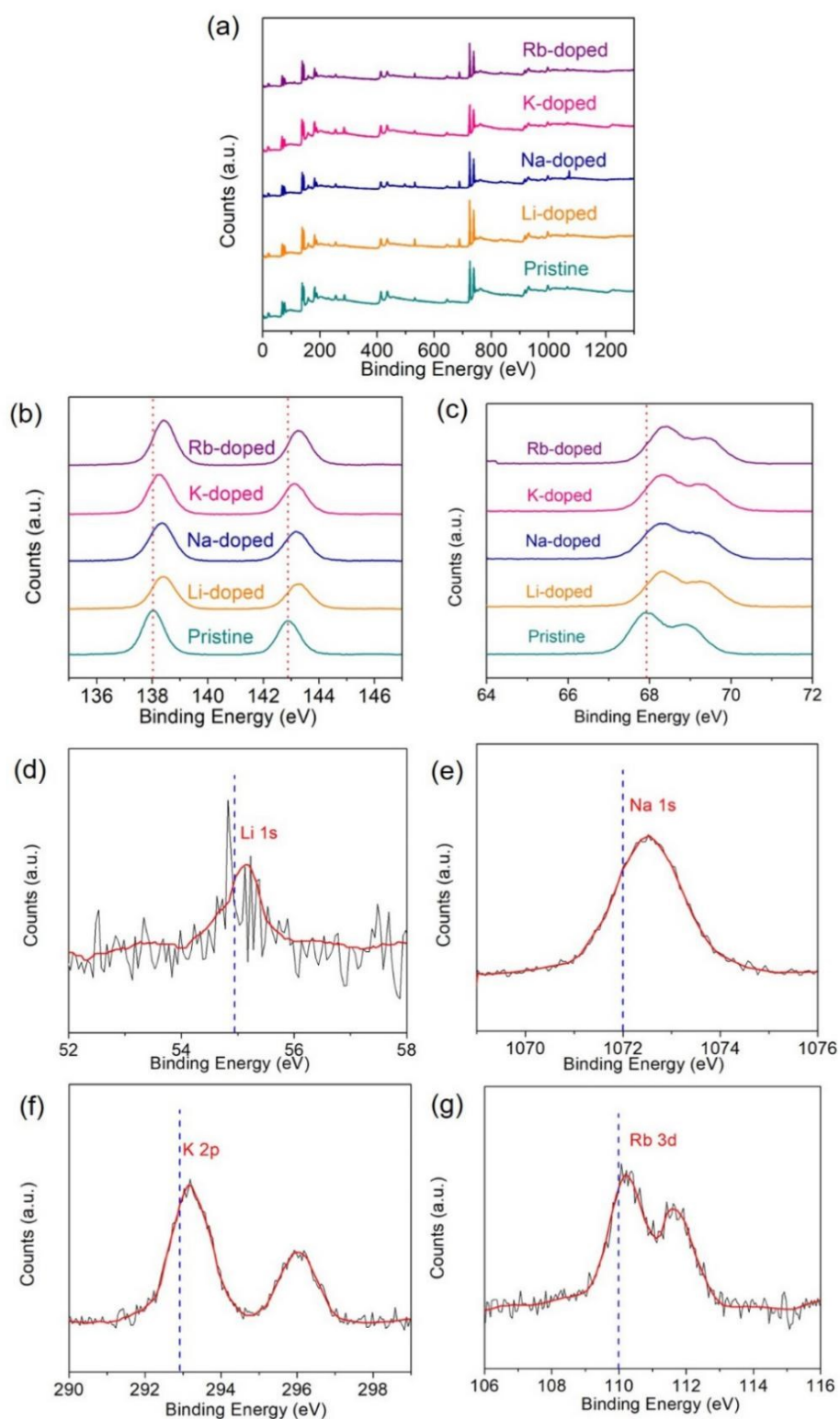


Figure S4. (a) High-resolution XPS spectra of pristine CsPbBr_3 and $\text{Cs}_{1-x}\text{A}_x\text{PbBr}_3$ perovskites. XPS spectra of (b) Pb 4f, (c) Br 3d, (d) Li 1s, (e) Na 1s, (f) K 2p, (g) Rb 3d. (d-g) The blue dash lines exhibit the standard electron binding energies of corresponding alkali metal ions.

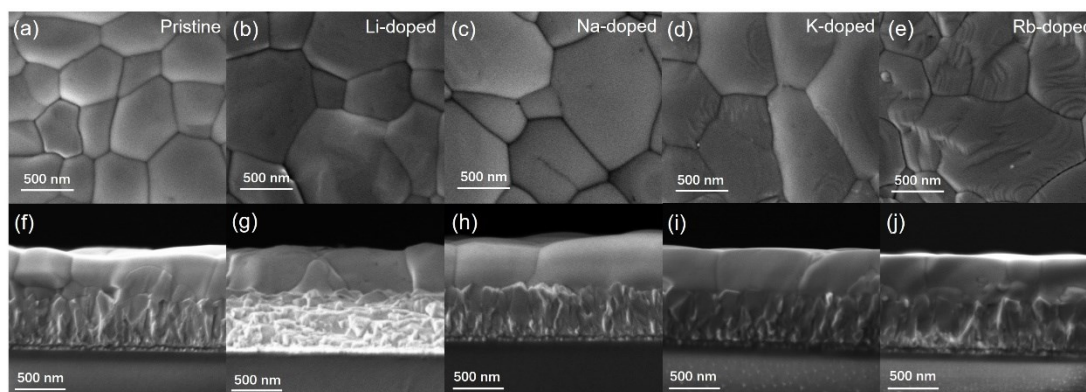


Figure S5. Morphological characteristics of pristine CsPbBr_3 and $\text{Cs}_{1-x}\text{A}_x\text{PbBr}_3$ perovskite films. (a-e) Top-view and (f-j) cross-section SEM images of (a,f) pristine CsPbBr_3 and the perovskite doped with (b, g) Li^+ , (c, h) Na^+ , (d, i) K^+ , (e, j) Rb^+ ions with optimal doping concentrations, respectively.

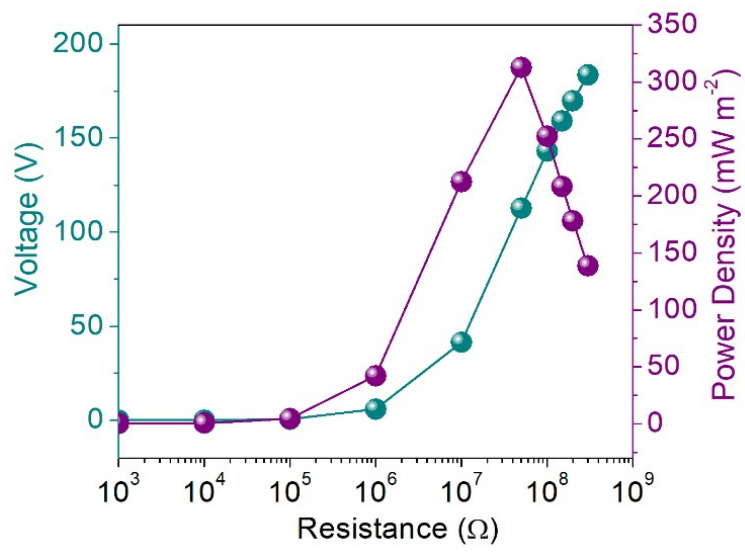


Figure S6. Voltage and power density outputs of FTO/CsPbBr₃-PVDF/Ag TENG at various external load resistances.

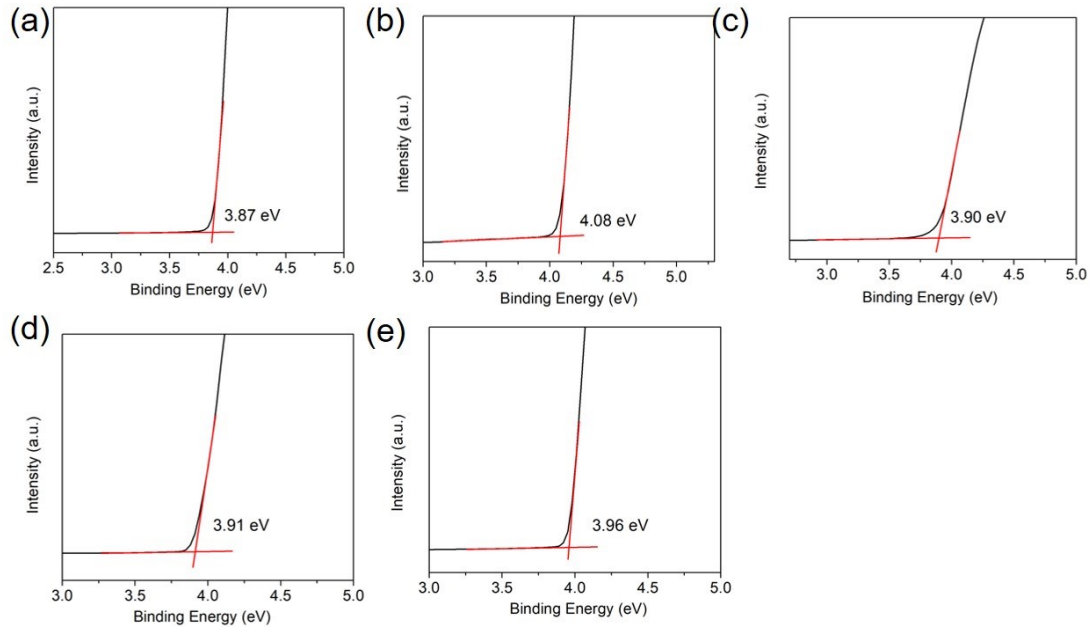


Figure S7. The ultraviolet photoelectron spectroscopy (UPS) spectra of (a) CsPbBr₃, (b) Cs_{0.99}Li_{0.01}PbBr₃, (c) Cs_{0.95}Na_{0.05}PbBr₃, (d) Cs_{0.90}K_{0.10}PbBr₃, (e)Cs_{0.85}Rb_{0.15}PbBr₃ perovskite films.

Theoretically, the work function can be calculated from UPS spectra according to the following equation: $W_F = h\nu + E_{\text{cutoff}} - E_{\text{Fermi}}$, where $h\nu$ is the exciting source and accurate, E_{Fermi} is also easy to demarcate from the differential of Fermi edge (Surf. Interface Anal. 26 (1998) 642-649). E_{cutoff} is relatively difficult to accurately demarcate due to the formation mechanism of the cutoff edge of secondary electron. Therefore, the fit error of W_F is mainly stemmed from the fit error of E_{cutoff} , which can be diminished within $\pm 0.01\text{eV}$ to the great extent (Phys. Examination Test. 25 (2007) 21-23), and thus we give the error bar of $\pm 0.01\text{eV}$.

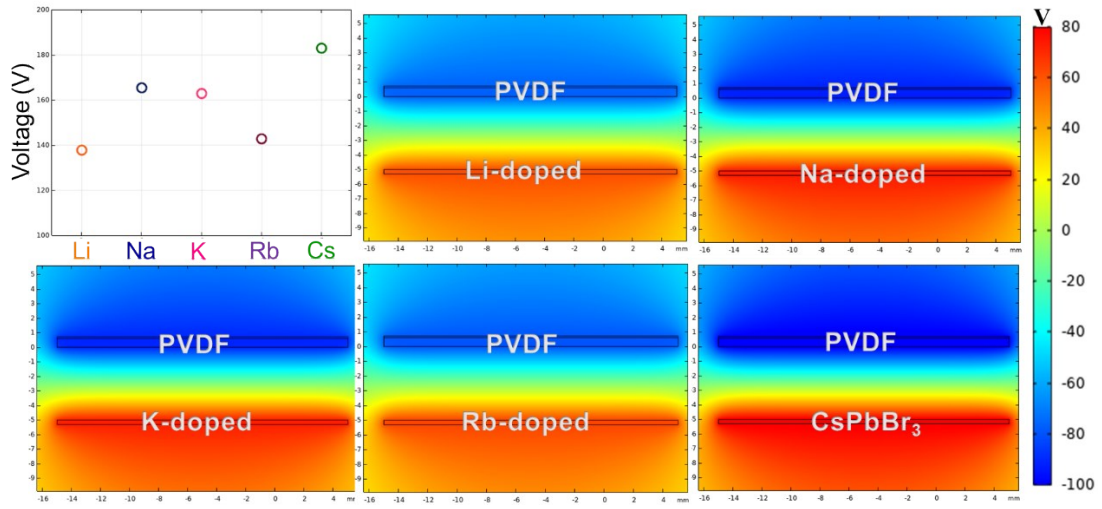


Figure S8. Simulated results of output potential difference between various Cs_{1-x}A_xPbBr₃ perovskites with optimal doping contents and their electrical potential distribution.

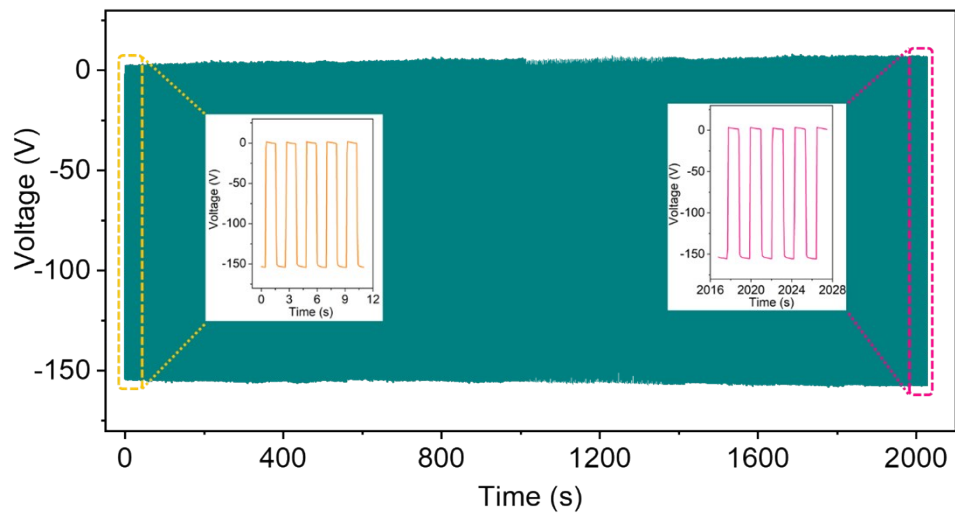


Figure S9. Durability test of the $\text{Cs}_{0.95}\text{Na}_{0.05}\text{PbBr}_3$ -PVDF TENG over 1000 cycles at ambient atmosphere.

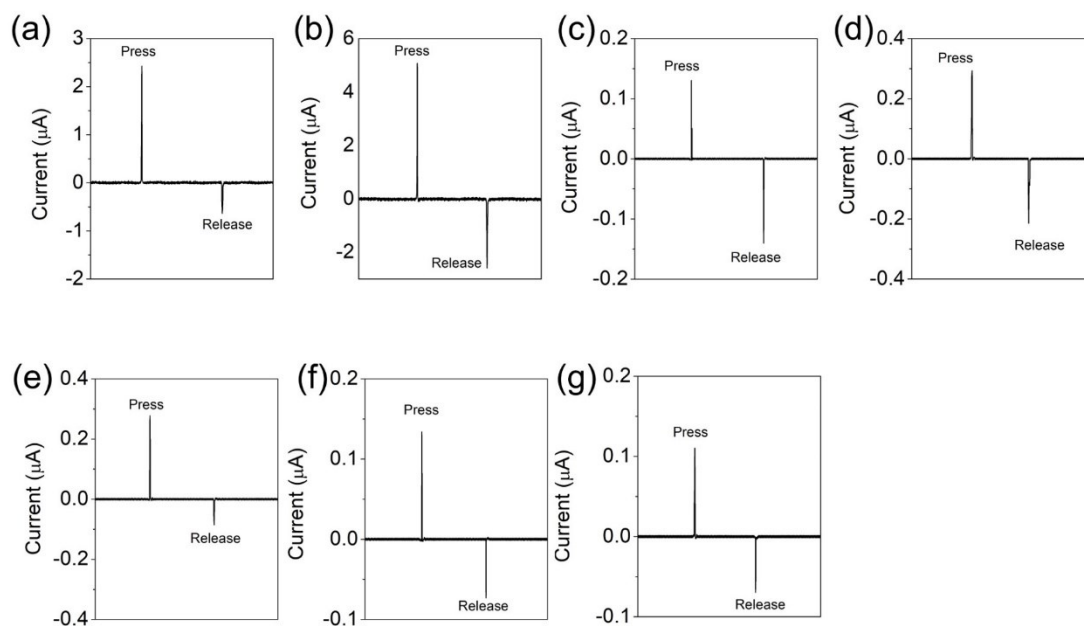


Figure S10. Triboelectric behaviors of the selected polymers. Triboelectric current signals of TENGs with (a) top PTFE-bottom PVDF, (b) top PVDF-bottom PDMS, (c) top PDMS-bottom PE, (d) top PE-bottom PC, (e) top PC-bottom PET, (f) top PET-bottom PI, and (g) top PI-bottom nylon pairs. Positive and negative signals obtained upon pressing or releasing indicate the larger electron affinity of the top polymer than the bottom one.

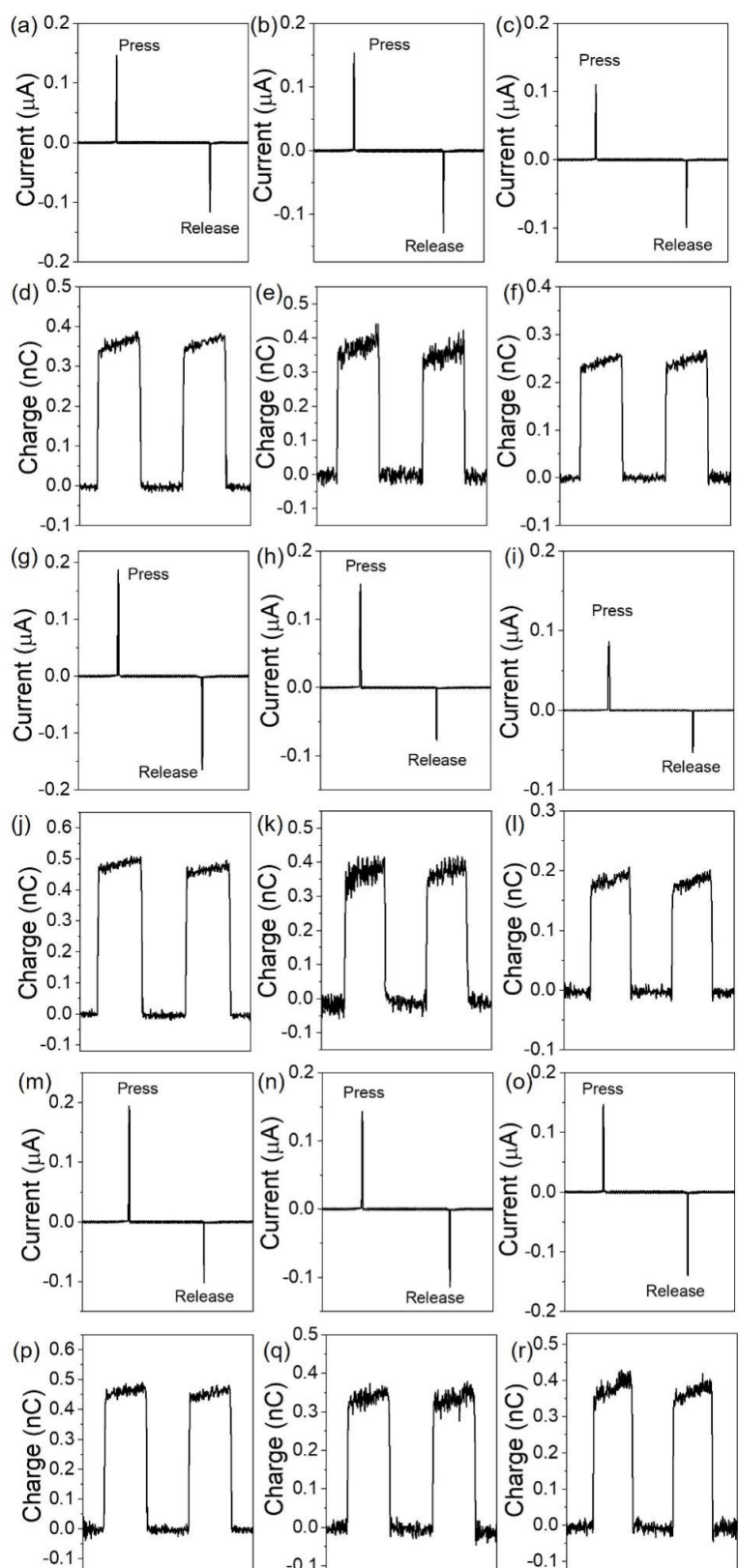


Figure S11. Triboelectrification behaviors of the $\text{Cs}_{1-x}\text{A}_x\text{PbBr}_3$ perovskites with (a-f) the second, (g-l) the third, (m-r) the fourth doping contents. Triboelectric current and

transferred charge signals of TENGs with (a,d,g,j,m,p) top Li doped-bottom Rb doped, (b,e,h,k,n,q) top Rb doped-bottom K doped, (c,f,i,l,o,r) top K doped-bottom Na doped pairs. Positive and negative signals were obtained upon pressing and releasing motions, indicating the larger electron affinity (more negative) of the top perovskite than the bottom one.

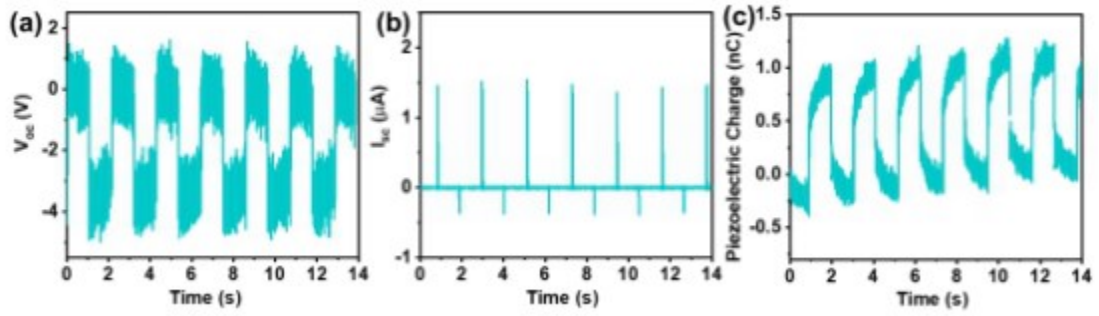


Figure S12. Piezoelectric behaviors of the FTO-PVDF/Ag device via keeping the contact status of the two counterparts.

Piezoelectric output with V_{oc} of 3 V, I_{sc} of 1.5 μA , and Q_{sc} of 1 nC are obtained for FTO/PVDF/Ag device. The low piezoelectric signals indicate little effect of piezoelectric polarization of PVDF on triboelectric output performance.

Table S1 Root mean square values of $\text{Cs}_{1-x}\text{A}_x\text{PbBr}_3$ films with various doping ions.

RMS* (nm) Doping concentration	Li⁺	Na⁺	K⁺	Rb⁺
0.01	38.6	31.5	40.1	NA
0.05	38.9	35.7	40.6	38.8
0.1	41	37.1	48	41.2
0.15	59.3	39.3	49	41.5
0.2	NA	NA	NA	42.9

*Root mean square (RMS)

Table S2 Summarized triboelectric charge density of the alkali metal ions, alkaline earth ions dopents and halogen regulation of perovskite TENGs.

Perovskite	V_{oc} (V)	E_m^* (μJ) ($R_{ex}=50M\Omega$)	σ (nC/m^2)**	Ref.
CsPbBr₃	182	13.6	322.14	This work
Cs_{0.99}Li_{0.01}PbBr₃	128	8.5	226.56	This work
Cs_{0.85}Rb_{0.15}PbBr₃	135	9.5	238.95	This work
Cs_{0.90}K_{0.10}PbBr₃	152	11.4	269.04	This work
Cs_{0.95}Na_{0.05}PbBr₃	158	12.4	279.66	This work
CsPb_{0.93}Sr_{0.07}Br₃	127	7.8	224.79	[1]
CsPb_{0.97}Ca_{0.03}Br₃	138	8.5	244.26	[1]
CsPb_{0.99}Mg_{0.01}Br₃	142	11.1	251.34	[1]
CsPb_{0.91}Ba_{0.09}Br₃	222	15.9	392.94	[1]
CsPbCl₃	257	16.53	454.89	[2]
CsPbI₂Br	225	14.5	398.25	[2]

* E_m : Maximum possible output energy per “press-release” cycle
** σ : Surface triboelectric charge density, calculated by $V_{oc} = \sigma x / \epsilon_0$

References

- [1] Y. Wang, X. Yang, X. Yu, J. Duan, Q. Yang, Y Duan, Q. Tang, *Nano Energy*, 2020, **77**, 105280.
- [2] X. Yu, Y. Wang, J. Zhang, J. Duan, X. Yang, L. Liu, Q. Tang, *J. Mater. Chem. A*, 2020, **8**, 4299.